

Functionalized Carbon Material in Cement-Based Composites, a Multivariate Approach

*Original*

Functionalized Carbon Material in Cement-Based Composites, a Multivariate Approach / Amata, Carlo; Panizzi, Simone; Farinini, Emanuele; Pavese, Matteo; Lavagna, Luca. - In: JOURNAL OF COMPOSITES SCIENCE. - ISSN 2504-477X. - ELETTRONICO. - 10:3(2026), pp. 1-18. [10.3390/jcs10030141]

*Availability:*

This version is available at: 11583/3009855 since: 2026-04-14T09:40:29Z

*Publisher:*

MDPI

*Published*

DOI:10.3390/jcs10030141

*Terms of use:*

This article is made available under terms and conditions as specified in the corresponding bibliographic description in the repository

*Publisher copyright*

(Article begins on next page)



Article

# Functionalized Carbon Material in Cement-Based Composites, a Multivariate Approach

Carlo Amata <sup>1</sup>, Simone Panizzi <sup>1</sup>, Emanuele Farinini <sup>2</sup>, Matteo Pavese <sup>1</sup> and Luca Lavagna <sup>1,\*</sup>

<sup>1</sup> Department of Applied Science and Technology, Politecnico di Torino, Corso Duca degli Abruzzi 24, 10129 Torino, Italy; carlo.amata@polito.it (C.A.); simone.panizzi@studenti.polito.it (S.P.); matteo.pavese@polito.it (M.P.)

<sup>2</sup> Department of Pharmacy, University of Genova, Viale Cembrano 4, 16148 Genova, Italy

\* Correspondence: luca.lavagna@polito.it

## Abstract

This study investigates the synergistic effect of functionalized carbon nanotubes (CNTs), graphene nanoplatelets (GNPs), and carbon fibers (CFs) on the mechanical performance of cement-based composites through a multivariate optimization approach. All carbon allotropes were covalently functionalized via acid treatment to enhance dispersion and interfacial bonding with the cement matrix. A face-centered central composite design (FCCD) combined with response surface methodology (RSM) was employed to systematically evaluate the influence of the three reinforcements, each varied between 0.033 wt.% and 0.067 wt.%, with a total carbon content not exceeding 0.2 wt.% of cement. The statistical analysis revealed a negligible correlation between reinforcement content and flexural strength (explained variance  $\approx$  1%), whereas fracture energy and compressive strength showed stronger dependencies, with explained variances of 25% and 66%, respectively. The maximum experimental fracture energy reached 18.1 J, corresponding to an increase of nearly 800% compared to plain cement, obtained at the highest combined reinforcement content. Compressive strength improved up to 48 MPa ( $\approx$ 32% higher than the reference), with the model predicting potential enhancements up to 40% under optimized compositions. The regression analysis highlighted the dominant role of quadratic and interaction terms, indicating that mechanical performance is governed more by synergistic effects than by the linear contribution of individual components. These findings demonstrate that controlled co-dispersion of multiple functionalized carbon allotropes enables significant enhancement of cement mechanical properties at very low total carbon contents, providing a cost-effective strategy for the design of high-performance cementitious composites.

**Keywords:** carbon nanotubes; graphene nanoplatelets; carbon fibers; multivariate optimization; response surface methodology; synergistic effect; cement-based composites



Academic Editor: Jiunn Jer Hwang

Received: 28 January 2026

Revised: 19 February 2026

Accepted: 4 March 2026

Published: 6 March 2026

**Copyright:** © 2026 by the authors.

Licensee MDPI, Basel, Switzerland.

This article is an open access article distributed under the terms and

conditions of the [Creative Commons Attribution \(CC BY\)](https://creativecommons.org/licenses/by/4.0/) license.

## 1. Introduction

Cement-based materials are essential for the construction industry, providing the foundation for creating vital infrastructure [1,2]. Their pervasiveness in the construction sector highlights the need for continuous research aimed at improving their properties and performance. Despite their versatility and robustness, traditional cement materials exhibit significant challenges in terms of durability in harsh environmental conditions. Addressing this issue is crucial for developing safer and longer-lasting construction materials. Moreover, increasing the duration and performance of structures based on cementitious materials also has a very positive impact on their overall environmental impact [3].

Cementitious matrix composites, which incorporate various reinforcements such as fibers and nanomaterials, have emerged as a promising solution to improve strength, safety and durability [4–8]. Over the past two decades, it has been known that carbon-based nanomaterials also have great potential for self-monitoring cement-based structures [9,10]. As stressed by Chung [11], these materials could enhance the ability of cementitious structures to autonomously monitor deformation and damage, foreshadowing advanced applications in the construction field. Recent updates on nanomaterials in cementitious systems have emphasized the importance of surface chemistry, particle size, and interfacial interactions in determining performance enhancement [12].

Although it is clear that the use of carbon allotropes—and nanomaterials in general—in cement composites can offer multiple benefits, it cannot be overlooked that the integration of carbon-based nanomaterials, such as CNTs and GNPs, into cementitious matrices presents significant difficulties [13]. Carbon-based materials like CNTs tend to agglomerate, leading to non-uniform dispersion within the cement matrix. Such inhomogeneous distribution can reduce their effectiveness in enhancing the mechanical properties and durability of the composite. Additionally, the hydrophobic nature of carbon-based materials hinders their compatibility with the hydrophilic cement matrix, resulting in poor interfacial adhesion. This weak bonding can adversely affect load transfer and the overall cohesion of the composite material [14,15].

As a general rule, it can be affirmed that carbon allotropes can increase the strength, toughness, and electrical conductivity of cement-based materials only if they are surface-modified and properly dispersed. Previous works from some of the authors on cement containing functionalized carbon allotropes confirm this hypothesis [16–18], as do some other literature papers that strongly suggest that functionalization of carbon allotropes is an important factor to guarantee a proper dispersion and a strong bond with cement paste [19]. There are various methods for the functionalization of CNTs and GNPs, broadly categorized into covalent and non-covalent functionalization. Covalent methods, such as chemical and electrochemical functionalization, introduce functional groups by modifying the lattice structure of carbon materials, thus providing more stable and durable bonds. In contrast, non-covalent methods preserve the original molecular structure of the nanotubes and graphene ( $sp^2$  hybridization of the carbon atoms), adding functional groups with less robust bonds. Some authors suggest that electrochemical and photochemical functionalization offer more accurate control compared to chemical methods [20,21]. Advanced dispersants and surfactant architectures have been developed to improve CNT stabilization in aqueous media, thereby facilitating their effective incorporation into cementitious matrices [22]. In the case of CFs, as mentioned by Shiba et al. [23], the functionalization methods differ mainly in their impact on the fiber surface and in the stability of the bonds created. Similarly to what happens with CNTs and GNPs, chemical and electrochemical oxidation introduces functional groups such as  $-COOH$  and  $-OH$ , improving adhesion with a potential polar environment; however, it can cause structural defects. In contrast, plasma treatments and coatings with metal oxides (e.g.,  $SiO_2$ ,  $TiO_2$ ) better preserve the integrity of the fibers, offering greater stability and protection against oxidation and thermal degradation. However, coatings are more expensive and complex to produce.

In order to guarantee both the dispersion in aqueous media and the bonding with cement paste, several functionalization and dispersing strategies were proposed in the literature [22–28]. Kang et al. [25] demonstrated that cement-composites samples containing acid-treated Multi Walled Carbon Nano Tubes (MWCNTs) showed a 30% increase in compression strength compared to control samples, along with a reduction in porosity. Wang et al. [26] showed that adding graphene nanoplatelets (GNPs) to cement, previously dispersed in an aqueous solution using a dispersing agent (methylcellulose) and ultrasoni-

cation, increased the compression strength of samples by 3–8% compared to cement without GNPs. This improvement was particularly noticeable in the short-term samples (7 days), with an increase in flexural strength ranging from 15% to 24%. With respect to CFs, Zhao et al. [29] demonstrated a positive effect even without functionalization. In fact, adding 0.6% carbon fibers by volume raises the compression strength from 35 MPa to 43 MPa representing a 22% increase compared to the sample without CFs. Furthermore, with CF content of 1.5% by volume, there was a 29% increase in splitting tensile strength. Other authors used functionalized carbon fibers, for instance Han et al. [27] reported gains in flexural strength for both 3 mm and 6 mm long fibers, after subjecting them to hydrophilic surface modification. For samples containing 0.8% of 3 mm long carbon fibers, flexural strength increased by up to 18% and with 6 mm fibers 22%. Compression strength saw an improvement of around 20% for both 3 mm and 6 mm fibers, after 28 days of curing. In an interesting study conducted by Li et al. [30], it was observed that an optimal ultrasonic dispersion of CNFs significantly enhanced the mechanical performance of UHPC, increasing the maximum flexural stress by up to 7.3% and the maximum flexural strain by up to 63%, due to a stronger CNF–CSH interface and a denser microstructure. Another study, by Mansouri Sarvandani et al. [19], highlighted that adding 0.1–0.2% by weight of acid functionalized multi-walled carbon nanotubes (MWCNTs–COOH) to cement mortars showed significant improvements in compression and flexural strength in both calcareous and sulfate-rich curing environments.

One of the most effective methods for covalent functionalization involves treating carbon materials with acid solutions, such as nitric acid or a mixture of nitric and sulfuric acid. This process introduces functional groups on their surface, altering the hybridization of a small percentage of carbon atoms from  $sp^2$  to  $sp^3$  through the addition of carboxyl or hydroxyl groups [16,31]. The resulting functional groups provide an improved compatibility with the cement matrix, promoting better dispersion in water and better chemical interaction. Although a large body of the literature has focused on individual carbon nanomaterials—particularly graphene oxide—the combined and multivariate optimization of different carbon allotropes within the same cement matrix remains comparatively less explored [32–35].

Despite these advancements in functionalization and dispersion of carbon-based materials in cement and concrete, the literature lacks systematic studies that explore the optimal simultaneous incorporation of all these carbon-based materials in cement-based composites. The present study addresses this gap by employing a multivariate approach for the experimental planning through design of experiments (DoE). For the purpose of the present study, a face-centered central composite design (FCCD) was considered to systematically investigate the effects of different concentrations of CNTs, GNPs, and CFs on the mechanical properties of cement composites. The FCCD design is a variant of the CCD (central composite design). FCCD is particularly useful in studies involving experimental optimization [36]. Its most notable features include the requirement of three levels for each factor (or independent variable), enabling the estimation of quadratic terms. This is essential for providing a comprehensive and accurate description of phenomena and for evaluating relative maxima in response outputs. Moreover, since the experimental effort required to prepare specimens and conduct testing is demanding in terms of both materials and time, FCCD aligns perfectly with the needs of research as it allows for reducing the number of experiments compared to a one-variable-at-a-time approach. This experimental approach not only allows for identifying and understanding the interactions between independent variables but also determines the optimal conditions for maximizing the desired responses [37]. Through response surface analysis [38], this study also provides deeper insights into the dynamics of the studied system, contributing to process

efficiency improvement and the development of higher-performing and more durable construction materials.

## 2. Materials and Methods

### 2.1. Materials

Multi-walled carbon nanotubes (CNTs), Nanocyl7000, produced through Chemical Vapor Deposition (CVD), were purchased from Nanocyl (Sambreville, Belgium). The producer declares an average diameter around 9.5 nm, an average length of 1.5  $\mu\text{m}$ , a purity of 90%, and a surface area of 250–300  $\text{m}^2/\text{g}$ . Graphene nanoplatelets (GNPs) grade 4 were purchased from Cheaptubes (Grafton, VT, USA). These nanoplatelets consist of small stacks of graphene sheets, each with an overall thickness of approximately 3–10 nanometers. The producer declares an average X and Y dimension  $> 2 \mu\text{m}$ , an average thickness between 8 and 15 nm, a purity of 97% and a specific surface area of 500–700  $\text{m}^2/\text{g}$ .

The carbon fibers (CFs) used in this research were purchased from Toho-Tenax (Tokyo, Japan); they are 6 mm in length and 7  $\mu\text{m}$  in diameter, with a tensile strength of 4 GPa and Young's modulus of 225 GPa. The cement used to produce the samples was Portland cement 52.5 R produced by Buzzi-Unicem (Casale Monferrato, Italy). For the functionalization of carbon-based materials, 98% sulfuric acid ( $\text{H}_2\text{SO}_4$ ), 65% nitric acid ( $\text{HNO}_3$ ), 30% hydrogen peroxide ( $\text{H}_2\text{O}_2$ ), and 97% sodium hydroxide (NaOH) were used; all the chemical reagents were supplied by Merck.

### 2.2. Functionalization of Carbon Materials

Functionalization of the surface of the carbon materials was achieved through acid treatment, with tailored procedures for each carbon allotrope. The chemical functionalization proposed in this study involved the use of strong acids to create defects that readily accommodate functional groups such as carboxylic ( $-\text{COOH}$ ) and/or hydroxyl ( $-\text{OH}$ ) groups [39]. To ensure comparability with previous studies [15–17], the same experimental conditions were applied. For CNTs, functionalization was performed by placing 1 g in a sonication bath (Sonica 2400MH series, Milano, Italy) containing 80 mL of sulfonitric acid (a mixture of 3 parts  $\text{H}_2\text{SO}_4$  98% and 1 part  $\text{HNO}_3$  65%) for 90 min. Similarly, 1 g of GNPs was functionalized in a sonication bath with 80 mL of sulfonitric acid for 60 min. For CFs, the functionalization process involved the sonication of a mixture of 1 g of CF and 80 mL of Piranha solution (3 parts  $\text{H}_2\text{SO}_4$  98% and 1 part  $\text{H}_2\text{O}_2$  30%) for 5 min. After the acid treatment, all carbon-based materials underwent a neutralization step with a basic solution containing NaOH. Each material was filtered using a fritted glass funnel and washed several times with deionized water to ensure complete elimination of residuals. Finally, the functionalized materials were dried in an oven at 100  $^\circ\text{C}$  overnight.

### 2.3. Characterization of Functionalized Carbon Materials

Thermogravimetric analysis (TGA) was performed using a Mettler Toledo MT-1600 (Greifensee, Switzerland) instrument. Samples of pristine and functionalized carbon materials were heated from 25  $^\circ\text{C}$  to 900  $^\circ\text{C}$  with a constant heating rate of 10  $^\circ\text{C}/\text{min}$  in a 50 mL/min air flow.

The morphology of the samples was examined by means of a FESEM Zeiss Merlin (Oberkochen, Germany).

### 2.4. Experimental Section

The procedure to prepare cement samples consists of the re-dispersion of carbon materials in water with an ultrasonic tip (VibraCell<sup>TM</sup>, Newtown, CT, USA) for 15 min at 100 W power. The slurry of carbon materials and water was then stirred mechanically for

several minutes while cement powder was slowly added. The cement paste, prepared at a water-to-cement ( $w/c$ ) ratio of 0.45 and containing different percentages of reinforcement, was then poured into suitable molds, kept for 24 h at 100% relative humidity, removed from the molds, and further cured immersed in tap water for a total curing time of 7 days. The carbon materials were added in a percentage varying from 0.033% to 0.066% by weight of cement; as shown in Table 1, the total carbon volume fraction ranged approximately between 0.15% and 0.30% with respect to the cement phase. These numbers were chosen in order to be able to compare the results with previously published research. Rectangular prismatic (parallelepiped) molds (Figure 1a) of  $20 \times 20 \times 80$  mm size were used for the cement composites, which were then mechanically tested to obtain flexural strength, fracture energy and compression strength.

**Table 1.** Experimental variables and corresponding levels used in the face-centered central composite design (FCCD) for optimizing the contents of functionalized carbon nanotubes (CNTs), graphene nanoplatelets (GNPs), and carbon fibers (CFs) in cement-based composites.

Variable ID	Variable Name	Levels		
		−1	0	1
$x_1$	CNTs (%)	0.033%	0.05%	0.066%
$x_2$	GNPs (%)	0.033%	0.05%	0.066%
$x_3$	CFs (%)	0.033%	0.05%	0.066%

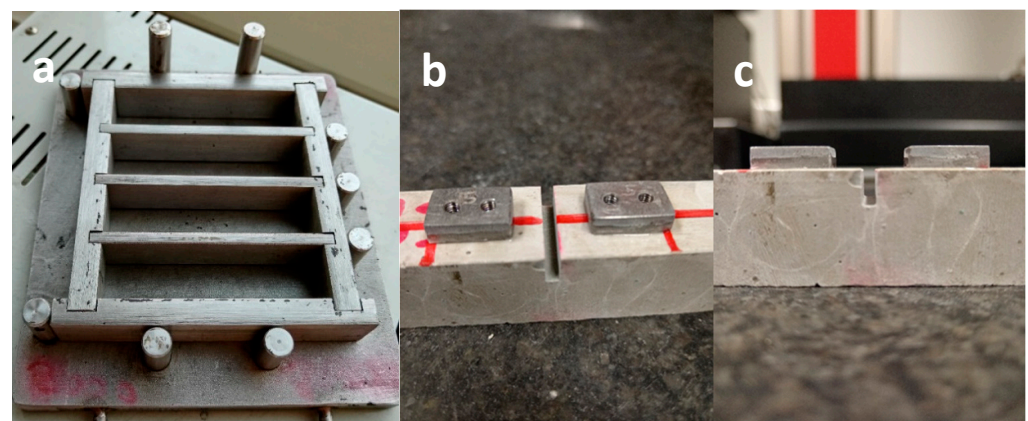


**Figure 1.** Mold used for the preparation of samples (a) and notched specimens ready for testing (b,c).

### 2.5. Mechanical Test and Characterization of the Sample

Adopting the operational methods previously described in a prior study [40], a single-column Zwick-Line z050 (Genova, Italy) with a load cell of 1 kN was used for the flexural tests. The bending strength and the fracture energy were measured following the standard JCI-001-2003 [41]. A three-point bending test was performed with a span of 65 mm in crack mouth opening displacement (CMOD) mode. The samples were prepared with a 6 mm deep and 2 mm wide notch in the middle of the sample (Figure 1b,c). An extensometer was placed on the two sides of the notch, and the CMOD was controlled at a fixed rate of 0.005 mm/min (Figure 2a). Compression tests were then performed in load control on one of the two halves produced by the flexural test, using the same machine with a 50 kN load cell (Figure 2b). The tests were conducted with a speed of 600 N/s with a preload of 20 N. Both the flexural and the compression test results were an average of at least four specimens.

The microstructure of the samples was examined by means of a Field Emission Scanning Electron Microscope (FESEM Zeiss Merlin (Oberkochen, Germany)). Both fracture

surfaces and cut specimens polished up to a 4000-grit paper were observed after metallization with platinum.

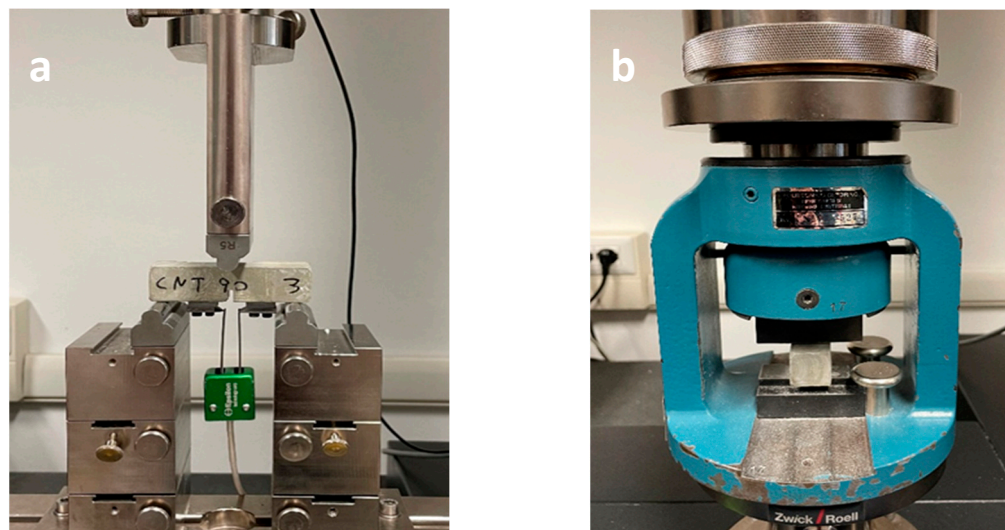


**Figure 2.** Experimental setup for flexural tests in CMOD (a) and for compression tests (b).

### 2.6. Statistical Model

This approach focused on three quantitative factors: the quantity of functionalized CNTs, GNPs, and CFs (percentage with respect to cement weight). These variables were investigated to determine their impact on mechanical performance (i.e., flexural strength, fracture energy and compression strength), with each variable tested at three levels (+1, 0, −1) to explore potential quadratic effects on the different responses. The levels are detailed in Table 1.

The levels were determined during the experimental design phase to ensure that the total amount of carbon-based material in the specimens never exceeded 0.2% by weight relative to the cement powder used in the mix design. For the statistical analysis of the data, CAT (Chemometric Agile Tool) software version 1.0 (2025) was employed.

The postulated full quadratic model includes a constant  $b_0$ , three linear terms  $b_1$   $b_2$   $b_3$ , three interactions terms  $b_{12}$   $b_{13}$   $b_{23}$ , and three quadratic terms  $b_{11}$   $b_{22}$   $b_{33}$ , as follows:

$$y = b_0 + b_1x_1 + b_2x_2 + b_3x_3 + b_{12}x_1x_2 + b_{13}x_1x_3 + b_{23}x_2x_3 + b_{11}x_1^2 + b_{22}x_2^2 + b_{33}x_3^2 \quad (1)$$

The experiments were selected using a face-centered central composite design (FCCD), requiring 15 experiments with the central point performed in triplicate to assess experimental variability. In total, 17 experiments were conducted to estimate 10 coefficients, with 7 degrees of freedom (d.o.f.). The experiments were performed in a randomized order to avoid any systematic effects [42]. To evaluate sampling and analytical variability, the mechanical properties were assessed on four subsamples for each condition.

## 3. Results

### 3.1. Thermogravimetric Analysis

The TGA analysis (Figure 3) shows a clear difference between the weight loss curves of pristine (orange lines) and functionalized materials (blue lines). Lower thermal stability in air was observed for all the functionalized carbons, with degradation starting at lower temperatures compared to the pristine samples. The reduction in degradation temperature is particularly evident in the case of CFs (Figure 3a) and CNTs (Figure 3b). Acid oxidation introduces oxygen-containing functional groups (e.g., −COOH and −OH) onto the carbon surface, locally disrupting the conjugated  $sp^2$  lattice and generating structural defects. The

presence of these oxygenated moieties reduces thermal stability for two main reasons: (i) the functional groups themselves are thermally labile and decompose at relatively low temperatures (typically between 150 and 400 °C), and (ii) the defect sites increase the reactivity of the carbon framework toward oxidative degradation. Consequently, the onset of mass loss shifts to lower temperatures after functionalization. Such behavior is widely reported for oxidized CNTs, graphene-based materials, and carbon fibers [20,21,43,44]. In particular, the degradation curve of oxidized carbon fibers (Figure 3a, blue line) begins at around 450 °C, compared to approximately 600 °C for pristine fibers, confirming the increased susceptibility to oxidation induced by surface treatment. A similar trend is observed for CNTs (Figure 3b), where an initial weight loss below 100 °C corresponds to adsorbed moisture, followed by a gradual mass loss between 100 °C and 400 °C attributed to the decomposition of surface oxygenated groups. The main oxidation step also occurs at a lower temperature compared to pristine CNTs, whose highly graphitic structure ensures higher thermal resistance. Oxidized GNPs (Figure 3c) display a comparable trend, with a slight but measurable anticipation of the degradation onset, consistent with the introduction of surface defects.

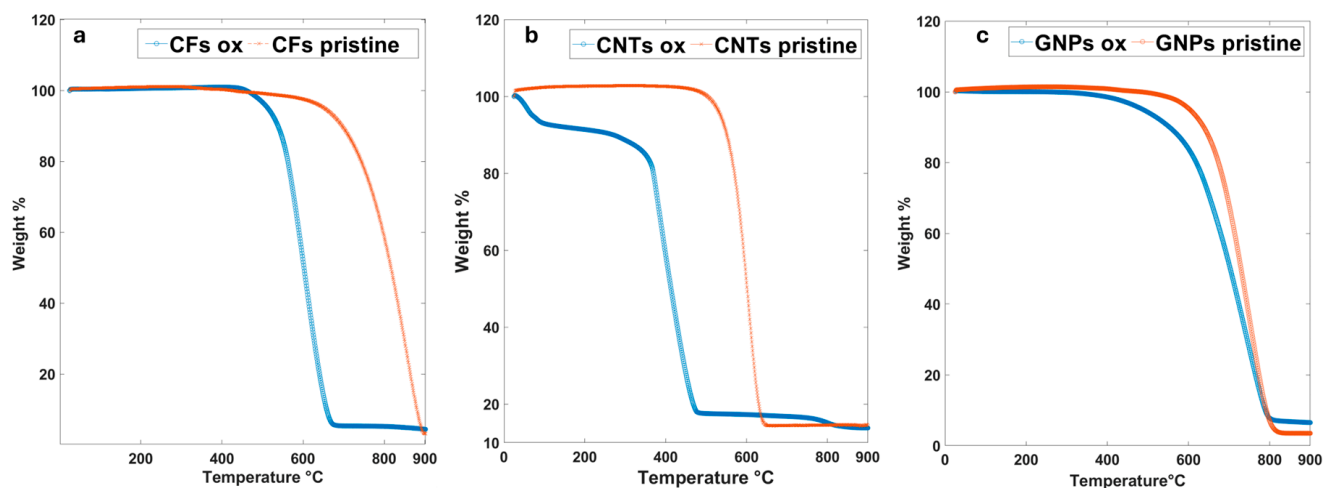


**Figure 3.** TGA curves of CFs (a), CNTs (b) and GNPs (c) in both the pristine and functionalized states.

Therefore, the reduction in oxidation temperature observed in functionalized samples should not be considered anomalous; rather, it represents indirect evidence of successful covalent functionalization and defect formation in the carbon structure

### 3.2. FESEM Characterization of Carbon Materials

Figure 4 shows representative FESEM images of pristine (a, c, e) and oxidized (b, d, f) carbon nanotubes, carbon fibers, and graphene nanoplatelets, respectively. No significant morphological differences are observed between pristine and functionalized materials at the investigated magnifications. The overall structural integrity of CNTs, CFs, and GNPs is preserved after the oxidative treatment, with no evidence of severe fragmentation, surface peeling, or dimensional alteration.

This behavior is consistent with the adopted functionalization procedure, which is known to introduce oxygen-containing groups mainly at the surface and defect sites without substantially modifying the bulk morphology of the carbon framework. Similar observations have already been reported in our previous works [16–18], where a detailed physicochemical characterization (including Raman spectroscopy, TGA, and surface analysis) confirmed that the oxidation process affects predominantly the surface chemistry rather than the structural morphology of the carbon materials.

For completeness, the full characterization of the functionalized carbon allotropes can be found in the above-cited references.

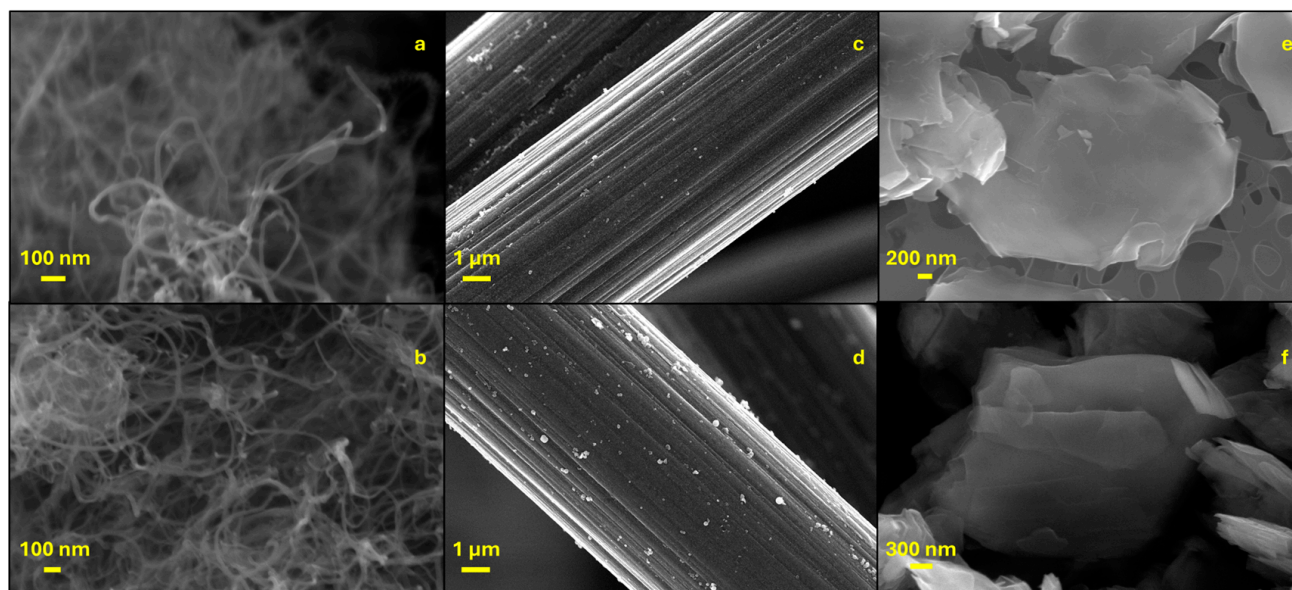


**Figure 4.** FESEM images from pristine (a) and oxidized (b) CNTs; pristine (c) and oxidized (d) CFs; and pristine (e) and oxidized (f) GNPs.

### 3.3. Mechanical Results

Table 2 reports the average values of flexural strength, fracture energy, and compression strength for all the tested samples. Based on the results of the performed experiments, it was possible to estimate both experimental and subsampling variability, which are also reported in terms of standard deviations. Experimental variability represents the reproducibility of single tests, whereas subsampling variability represents the internal heterogeneity of the specimens.

The data reported in Table 2 are shown in graphic form in Figure 5, where the comparison of flexural strength, fracture energy, and compression strength for samples C1 to C17 and the reference sample can be observed. Regarding flexural strength (Figure 5a), samples C17 and the reference exhibit the highest values, around 3.4 MPa, while most of the other samples have lower strength values, between 1.8 and 3.3 MPa. The error bars in this graph indicate the standard deviation of each set of samples. Regarding fracture energy (Figure 5b), all the tested samples have higher values than the reference. Notwithstanding the significant experimental variability, sample C8 stands out with the highest value, 18.1 J, with an increment of almost eight times, followed by C10, with a five-fold fracture energy increment. These results are consistent with a previous study where the fracture energy of cement samples composite containing 0.1% of functionalized carbon fibers was analyzed. In the present study, the fracture energy increases with the amount of functionalized CFs. Finally, in the compression strength results (Figure 5c), sample C6 reaches the highest compression strength, 48.1 MPa, followed by C7 and C10. The reference sample again displays the lowest value, with 36.3 MPa. The experimental variability in this case is smaller if compared to the other tests. The model was computed starting from the results shown in Table 2, allowing the observation of the response surface. This enabled the observation of the points within the experimental domain where the relative maxima for flexural strength, fracture energy, and compression strength were achieved.

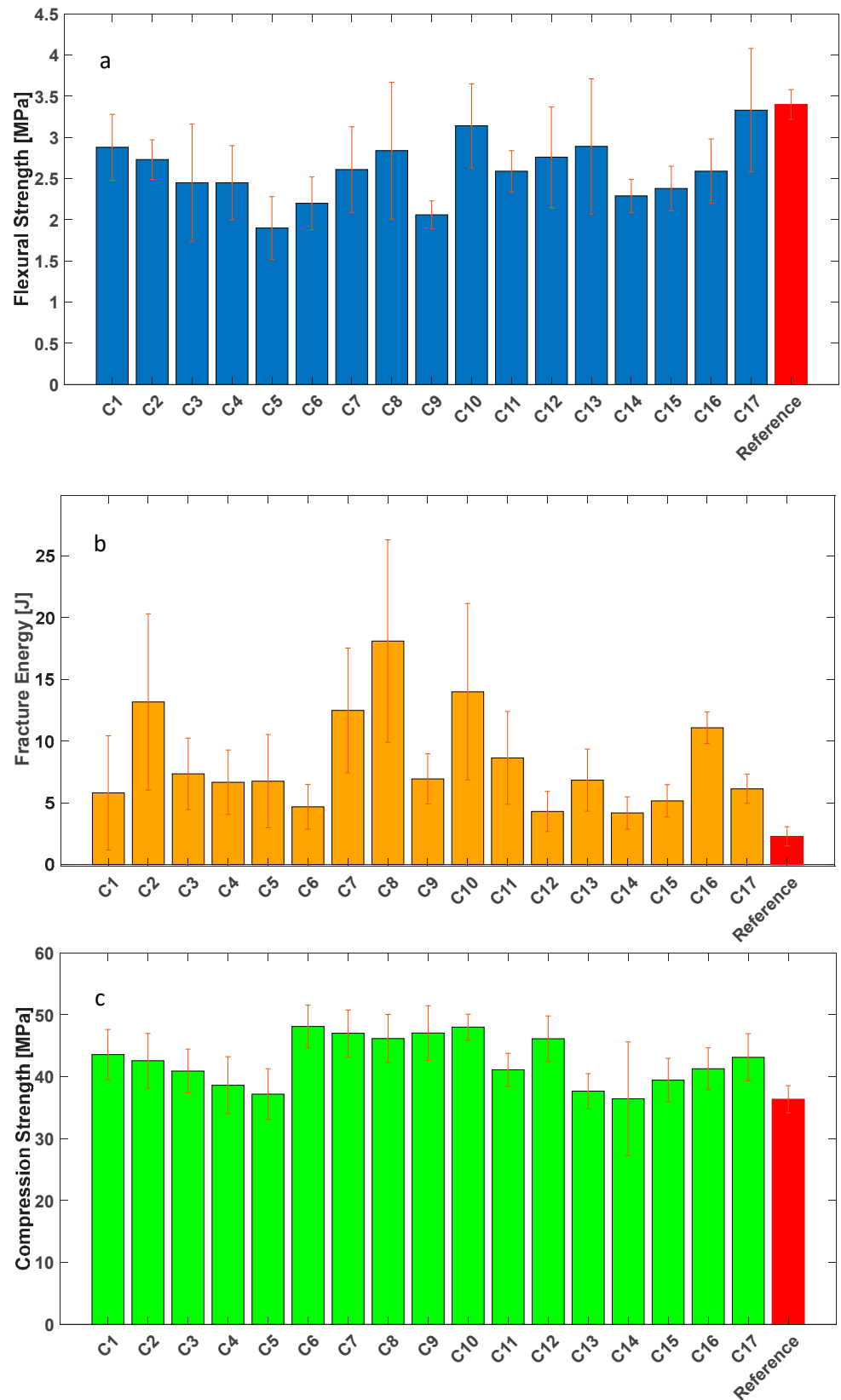


**Figure 5.** Bar charts showing the results of the mechanical tests for the flexural strength ((a) in blue), fracture energy ((b) in orange), and compression strength ((c) in green), with the reference values for each test (in red); the standard deviation is reported ( $N = 4$ ).

**Table 2.** Experimental matrix together with mechanical testing results are reported in the standard order; average values for flexural strength, fracture energy and compression strength are reported.

#	Experimental Matrix			Mechanical Results		
	$x_1$ CNTs	$x_2$ GNPs	$x_3$ CFs	$y_1$ Flexural Strength (MPa)	$y_2$ Fracture Energy (J)	$y_3$ Compression Strength (MPa)
R	-	-	-	3.40	2.30	36.3
1	-1	-1	-1	2.88	5.81	43.6
2	1	-1	-1	2.73	13.2	42.6
3	-1	-1	1	2.45	7.35	40.9
4	1	-1	1	2.45	6.67	38.6
5	-1	1	-1	1.90	6.76	37.2
6	1	1	-1	2.20	4.68	48.1
7	-1	1	1	2.61	12.5	47.0
8	1	1	1	2.84	18.1	46.2
9	-1	0	0	2.06	6.94	47.0
10	1	0	0	3.14	14.0	48.0
11	0	0	-1	2.59	8.64	41.1
12	0	0	1	2.76	4.30	46.1
13	0	-1	0	2.89	6.84	37.6
14	0	1	0	2.29	4.18	36.4
15	0	0	0	2.38	5.16	39.4
16	0	0	0	2.59	11.1	41.3
17	0	0	0	3.33	6.14	43.1
Experimental variability (3 d.o.f.)				0.50	3.18	1.9
Subsampling variability (46 d.o.f.)				0.47	4.23	4.3

### 3.4. FESEM Characterization of the Composites

In Figure 6a an image of sample C8 is shown, where it is possible to observe CNTs (yellow arrow) dispersed in a calcium silicate hydrate (C-S-H) matrix. The presence of CNTs well dispersed in a C-S-H matrix suggests that there is a good interaction between cement and functionalized CNTs. Figure 6b shows a carbon fiber with calcite (the larger particles) and calcium silicate hydrate (C-S-H) grafted on its surface. The presence of polar phases adhered to the surface of the carbon fiber is confirmation that the functionalization process facilitates the interaction between the fibers and the cement matrix.

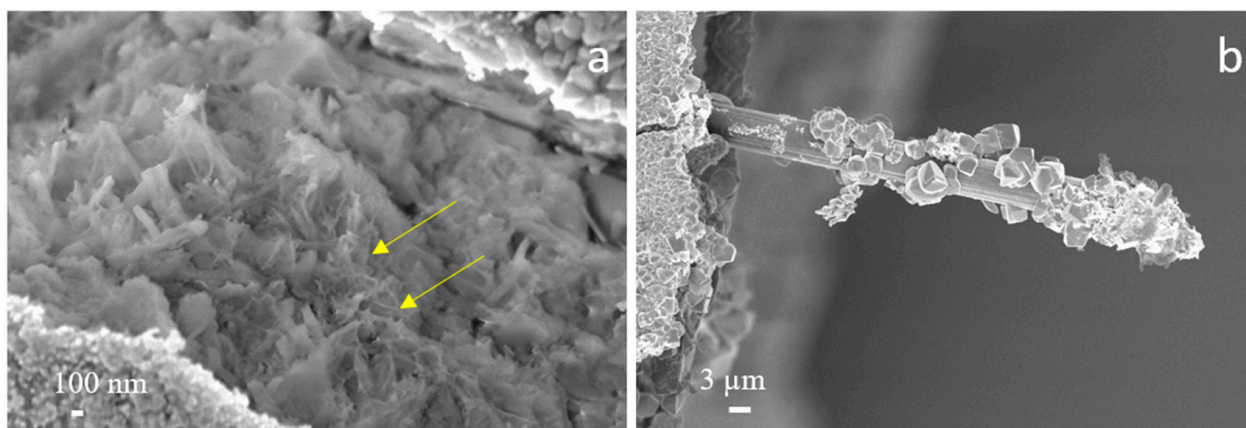


**Figure 6.** FESEM images showing carbon nanotubes embedded in the C-S-H gel (a) and a carbon fiber with C-S-H and calcite deposits (b).

3.5. Model

The modeling analysis performed on the results of flexural strength revealed that the explained variance (EV) for flexural strength is less than 1%. This very low EV indicates that variations in flexural strength are not significantly correlated with the amount of functionalized carbon allotropes added to the mixture. While this does not diminish the rigor of the experimental work, it suggests that the flexural strength results lack sufficient statistical significance to support meaningful conclusions. Therefore, we have chosen to exclude flexural strength from further discussion and focus on the mechanical properties that exhibit a stronger dependency on the carbon allotrope content.

Using the experimental results, a multiple linear regression (MLR) was carried out. Model coefficients are reported hereunder and in Figure 7; stars represent the statistical significance (*p*-value: \* = 0.05, \*\* = 0.01).

$$y_2 = 6.71 + 1.73x_1 + 0.63x_2 + 1.53x_3 - 0.39x_1x_2 - 0.04x_1x_3 + 3.00x_2x_3(*) + 4.72x_1^2 - 0.26x_2^2 - 2.04x_3^2$$

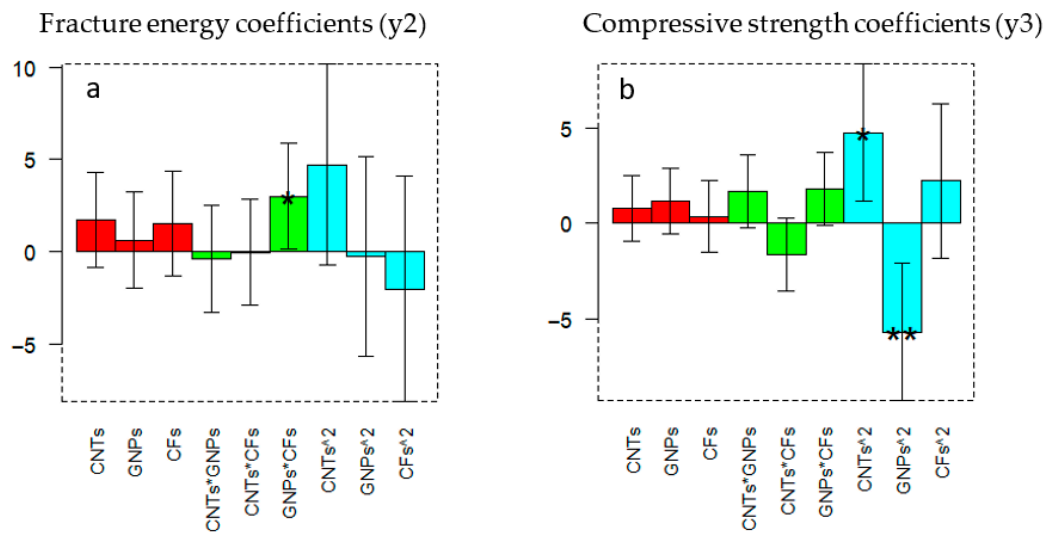


Figure 7. Coefficients of the multivariate analysis with error bars for fracture energy (a) and compression strength (b); stars represent the statistical significance.

Explained variance: 25%; residual SD: 3.45

$$y_3 = 41.97 + 0.78x_1 + 1.14x_2 + 0.35x_3 + 1.66x_1x_2 - 1.63x_1x_3 + 1.80x_2x_3 + 4.75x_1^2(*) - 5.73x_2^2(**) + 2.22x_3^2$$

Explained variance: 66%; residual SD: 2.29

The model for fracture energy shows a relatively low explained variance (25%), mainly due to the high standard deviations observed among specimens, which limit the model’s predictive capability. In contrast, the model for compression strength achieves an explained variance of 66%, indicating that compression strength represents a more predictable and consistent response compared to fracture energy.

The contour plots shown in Figure 8 are 2D graphical representations of the model prediction, where lines (contours) connect points of equal response values, illustrating how the output varies. To interpret them, it is necessary to identify the isoresponse lines corresponding to specific response levels and observe how these lines shift along the axes, thereby indicating which factor combinations yield higher or lower values.

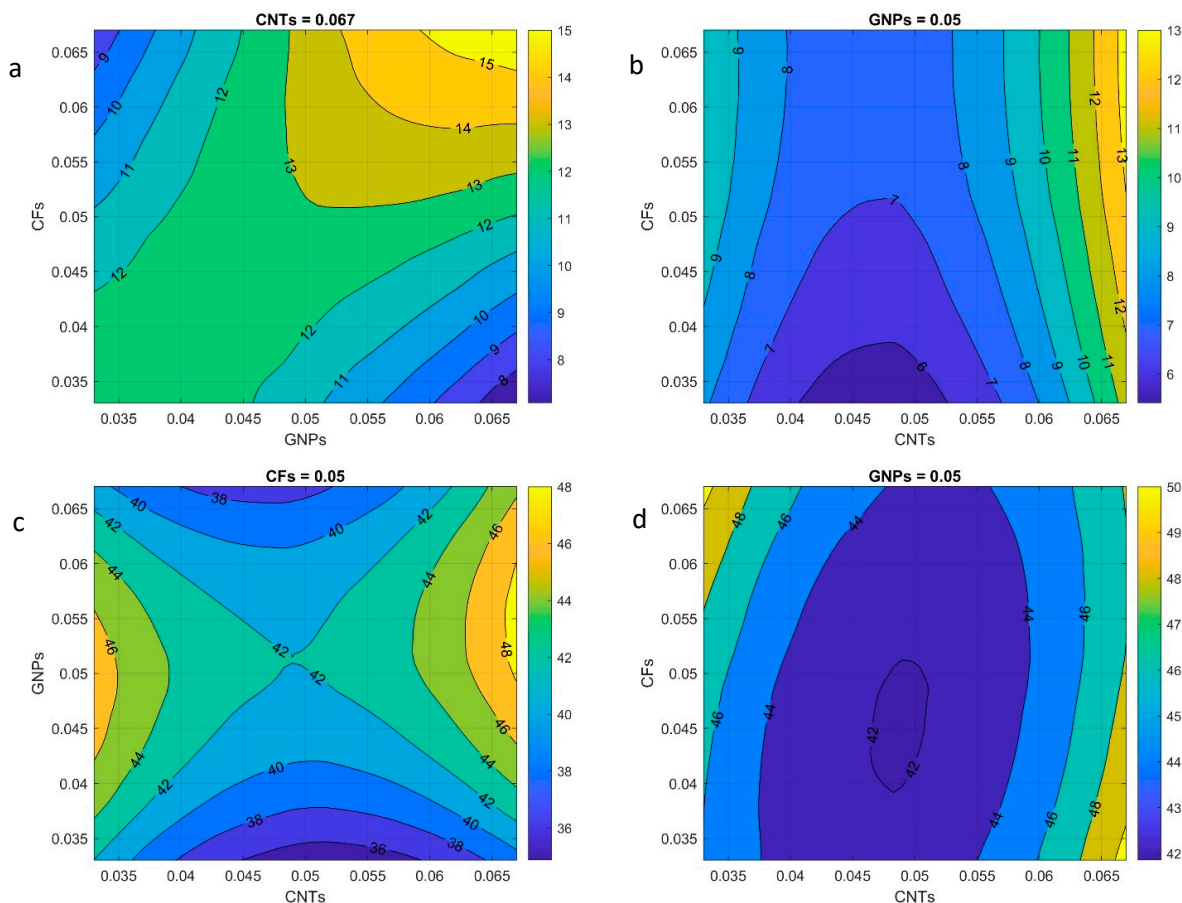


**Figure 8.** Contour plots for the responses of fracture energy (a,b) and compression strength (c,d).

Another method of representation of these results is the response surface (RS), depicted in Figure 9. All these graphical representations give the same information but require that one of the variables be fixed. In the case of Figure 8, the results are plotted for four cases: two fracture energy ( $y_2$ ) and two compression strength ( $y_3$ ) cases, where the fixed variable is either  $x_1$  (CNT content),  $x_2$  (GNP content), or  $x_3$  (CF content). Thus, for instance, in Figure 8a the plane  $x_2$ - $x_3$  is shown, with the isolines providing the information of the effect of the two variables on fracture energy predictions. Since the interaction between carbon fibers and graphene nanoplatelets is the most significant term for fracture energy, fixing CNTs allows a clearer visualization of this effect and of the location of the maximum on the contour plot. In Figure 8b the GNP concentration is fixed in order to show the CNT quadratic term, which is the second most statistically relevant. For compression strength, since the quadratic terms of both CNTs and GNPs are the most relevant, the shape of the surface can be most clearly represented when fixing CF (Figure 8c). Also, in Figure 8d, the curve for fixed GNP concentration is represented, showing the CNT-positive curvature indicated by the quadratic term. In Supplementary Information (Figures S1–S3), all the contour plot curves are presented.

In Figure 9, all the response surfaces are shown for the compression strength ( $y_3$ ) case. The curvature terms are evident, but also the linear and interaction terms can be inferred even if they are not statistically significant. In any case, these curves can be used to improve the knowledge and understanding of the behavior of the samples. In Supplementary Information (Figures S4 and S5), the equivalent figures for flexural strength and fracture energy are presented. Moreover, nine animations are uploaded that provide a clear graphical understanding of the behavior of the material.

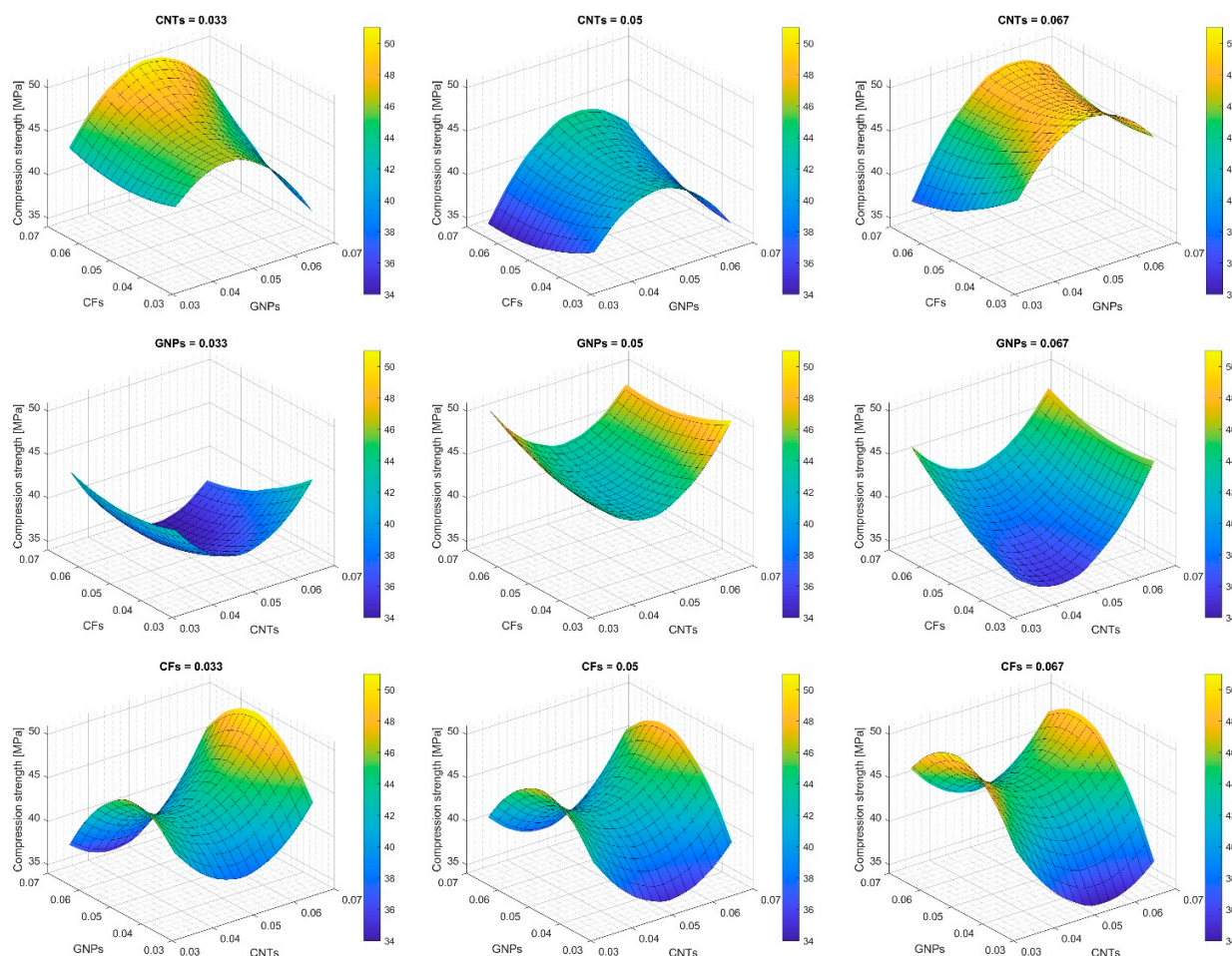


Figure 9. Response surfaces corresponding to experimental data for compression strength.

### 4. Discussion

The construction of a model and the subsequent generation of both contour plots (Figure 8) and response surfaces (Figure 9) allow coupling a precise statistical analysis with a facilitated graphical observation of experimental results.

In this paper, starting from a carefully designed set of experiments, we used a statistical model to draw conclusions on the effect of the simultaneous presence of CNTs, GNPs and CFs inside a cementitious matrix. The model gave the following information.

The explained variance of experimental results. This suggested that no statistical significance was present in flexural strength results (only 1% explained variance), and thus the variation in the results of these tests must be considered very carefully, and no certain conclusion can be drawn. This behavior suggests that flexural strength is not the most sensitive parameter for capturing the synergistic effects of the combined carbon reinforcements at such low volume fractions. Regarding fracture energy, the explained variance is not very high (25%), suggesting that some information on the synergistic effects of the different carbon materials can be obtained, but care must still be exercised in the analysis of the results. A better situation with compression strength is obtained, where the explained variance is 66%.

The effect of a single carbon material, while evident when added singularly to a cement matrix, becomes less straightforward when the synergy between the different carbon phases is considered. As shown in Figure 7, only a few of the fitted parameters are statistically significant, in particular, second-order parameters. This means that the interaction and quadratic terms are more important than linear ones, suggesting that the

co-dispersion of carbon materials and the physical–chemical interaction among them play an important role in determining the final composite properties.

The maximum predicted value for every test can be computed by the model, giving the optimal quantity of carbon material to use to guarantee the best results. However, it must be considered that this value has the weight of the explained variance, so it is significant only for compression strength and less so for fracture energy. In the case of fracture energy, the best results are obtained for the maximum amount of all three carbon allotropes (0.067% each, with a total carbon content of 0.2%). In the case of compression strength, instead, the maximum is obtained either for 0.067% CFs, 0.033% CNTs, and 0.052% GNPs or 0.033% CFs, 0.067% CNTs, and 0.052% GNPs.

A comparison with the literature, in particular with previous papers of the authors, can give some further information about these results.

Speaking about fracture energy, it must be first considered that the addition of even a small amount of carbon fibers in cement increases it greatly [17], while only nanotubes [16] or graphene nanoplatelets [18] do not significantly increase this property. A synergistic effect of CFs and either CNTs or GNPs was already observed by Lavagna et al. [40], with a positive interaction with CNTs and a negative one with GNPs. In the same paper, the effect of CFs, CNTs and GNPs seemed negative, showing no improvement with respect to cement, but probably due to some issue in dispersion. The maximum value of fracture energy observed with only CFs was around 10 J; with CFs and CNTs, it reached almost 17 J.

In this paper, we obtained 18.1 J, almost eight times the value for pure cement, even if the model prediction smooths this value to around 16 J, probably due to the high experimental variability. The results are thus consistent with previously published experiments. The interaction effect, however, shows some unexpected trends, since the CNTs\*CFs interaction coefficient, although not statistically significant, seems close to zero, and the GNPs\*CFs interaction coefficient is positive, contrary to what is suggested by [43]. This is most probably due to the complex interaction between all three carbon materials that modifies the trend typical for binary systems. Also, the cited papers [16–18,40] always contained 0.1% by weight of cement of carbon materials, while in this paper the total content varies between 0.1% and 0.2%, and the best results are obtained with 0.2%.

In the literature, some papers declare similar fracture energy improvements. For instance, Dalla et al. [45] obtained an improvement in fracture energy (CMOD) of 970% in mortar specimens with 1% of GNPs added, while the maximum increase they obtained in fracture energy with CNTs was an increase of 590% with a concentration of 0.4 wt.% of CNTs in the mortar. The increase in carbon content can thus have a positive effect on fracture energy results, even if at the expense of a higher material cost. In this paper, we tried to limit the total content in order to reduce the final cost of the material. Considering that cement has a cost around 100 €/ton and carbon materials have a cost of a few tens of euros per kilogram, 0.1% of carbon means an increase of a few tens of percent of the cost, which is not irrelevant at all in the construction sector; 0.4% of CNTs would double or triple the cement cost, which seems too much even for a material with significantly improved properties.

Overall, it seems clear that fracture energy is improved with the presence of carbon fibers, but that CNTs and GNPs have a positive synergistic effect. The complex interactions among the three carbon types are probably the reason for the not straightforward interpretation of the interaction factors.

Regarding compression strength, the interpretation of results is less clear-cut. All the carbon materials singularly increase the strength, even if GNPs have a less clear effect [16–18,40]. In [40], the synergistic effect is not clearly seen on compression strength, while in this work we observe a significant improvement in mechanical properties when CFs, CNTs and GNPs are added, as shown in Figure 5. In particular, the best experimental

result corresponds to an increase of 32% with respect to pure cement, while the model suggests that up to a 40% increase can be reached. In a study conducted by Abedi et al. [46], where a mortar containing a mix of 0.5% CNTs and 0.5% GNPs is investigated, the compression strength increases 28% after 7 days and 36% after 28 days, similarly to this work. Abedi et al. conclude that the incorporation of nanotubes and graphene in the cementitious composite leads to a denser and more homogeneous structure. A similar explanation was also given in [16,18] for the improvement of mechanical properties; in fact, while CFs are millimeter-sized, nanomaterials like CNTs and GNPs have a maximum size in the micrometer range, and they provide the reinforcing effect not only through their properties but also by improving cement phase nucleation and density. Also in this work, it is plausible to justify the results with an analogous reasoning; moreover, the model suggests a strong contribution to compression from CNTs and GNPs and a lower contribution from CFs, even if the coefficients are not statistically significant. Another interesting study conducted by Kanellopoulou et al. [47] shows that adding to the mortar a mix of CNTs treated with strong acids and carbon microfibers (CMFs) can lead to an increase in compression strength, with a gain of 49% in 28 days of curing; specimens that performed in this way contained 0.4% of CMFs and 0.05% of CNTs. Also in this case, the results are comparable with our results, even if the CFs' quantity is much higher than in this work.

From an economic perspective, considering a cement content of approximately 400 kg/m<sup>3</sup> and a maximum carbon addition of 0.2 wt.%, the total carbon requirement would be about 0.8 kg/m<sup>3</sup>. Assuming industrial-grade carbon fillers priced in the range of 30–50 €/kg, the additional cost would be approximately 24–40 €/m<sup>3</sup>. Although this increase may not be suitable for conventional mass concrete applications, it could be justified in high-performance, repair, or multifunctional structural elements where enhanced fracture resistance and durability are critical.

## 5. Conclusions

This study focuses on the use of statistical methods to facilitate the analysis of the synergistic effect of carbon fibers (CFs), carbon nanotubes (CNTs) and graphene nanoplatelets (GNPs) in a cement matrix. All the three carbon materials were added in percentages between 0.033% and 0.067%, with a total carbon content ranging from 0.1% to 0.2% by weight of cement. Carbon materials were first functionalized to guarantee a proper dispersion in water and subsequently in cement, as discussed in previous papers of the authors [15–17].

The research utilized a face-centered central composite design (FCCD) to systematically evaluate the effects of varying concentrations of these three reinforcements, thereby identifying the most influential variables for each response and quantifying the experimental noise associated with the analysis of each response. Results and key insights are outlined below. The statistical analysis provides information on the reliability of results, as shown by the explained variance. The coefficients of the multivariate analysis suggest which interactions are the most effective and which ones are statistically significant.

The model allows for the prediction of the maximum values for the measured properties. Regarding flexural strength, the explained variance of the results is very low, 1%, suggesting that no statistical interpretation of data is possible. The results for flexural strength ranged between 1.9 and 3.3 MPa, but no clear indication can be given on the effect of the three carbon materials on these properties. Regarding fracture energy, the explained variance is 25%. This value is not very high, due to the significant experimental variance in the results, but some conclusions can be drawn. Fracture energy reached its highest values at the maximum concentrations of all three reinforcements, with the coefficient of the multivariate analysis suggesting a particular positive correlation between CFs and GNPs. The best-performing composite achieved a fracture energy of 18.1 J, almost 800% higher

than the reference sample. Regarding compression strength, the explained variance is high, 66%. Compression strength showed notable improvements, with the model predicting the highest value at an intermediate amount of GNPs and either high CFs and low CNTs or low CFs and high CNTs, a result suggesting that high concentrations of both these components could lead to difficulties in dispersion and thus in defect formation. The best-performing composite achieved a compression strength of 48 MPa, 32% higher than the reference sample, with the model predicting a possible increase up to 40%.

**Supplementary Materials:** The following supporting information can be downloaded at: <https://www.mdpi.com/article/10.3390/jcs10030141/s1>, Figure S1: Contour plots for the responses of flexural strength; Figure S2: Contour plots for the responses of fracture energy; Figure S3: Contour plots for the responses of compression strength; Figure S4: Response surfaces relative to flexural strength; Figure S5: Response surfaces relative to fracture energy.

**Author Contributions:** Conceptualization, L.L. and M.P.; methodology, L.L., E.F. and M.P.; software, C.A., E.F. and M.P.; validation, L.L., C.A. and M.P.; formal analysis, S.P. and C.A.; investigation, C.A. and S.P.; resources, L.L.; data curation, C.A.; writing—original draft preparation, C.A., L.L. and M.P.; writing—review and editing, L.L. and M.P.; visualization, C.A. and M.P.; supervision, L.L.; project administration, M.P.; funding acquisition, M.P. and L.L. All authors have read and agreed to the published version of the manuscript.

**Funding:** This research received no external funding.

**Data Availability Statement:** The original contributions presented in this study are included in the article/Supplementary Material. Further inquiries can be directed to the corresponding author.

**Conflicts of Interest:** The authors declare no conflicts of interest.

## References

1. Nilimaa, J. Smart Materials and Technologies for Sustainable Concrete Construction. *Dev. Built Environ.* **2023**, *15*, 100177. [[CrossRef](#)]
2. Rodrigues, F.A.; Joekes, I. Cement Industry: Sustainability, Challenges and Perspectives. *Environ. Chem. Lett.* **2011**, *9*, 151–166. [[CrossRef](#)]
3. Pradhan, S.; Chang Boon Poh, A.; Qian, S. Impact of Service Life and System Boundaries on Life Cycle Assessment of Sustainable Concrete Mixes. *J. Clean. Prod.* **2022**, *342*, 130847. [[CrossRef](#)]
4. Arslan, M.E. Effects of Basalt and Glass Chopped Fibers Addition on Fracture Energy and Mechanical Properties of Ordinary Concrete: CMOD Measurement. *Constr. Build. Mater.* **2016**, *114*, 383–391. [[CrossRef](#)]
5. Liew, K.M.; Kai, M.F.; Zhang, L.W. Carbon Nanotube Reinforced Cementitious Composites: An Overview. *Compos. Part. A Appl. Sci. Manuf.* **2016**, *91*, 301–323. [[CrossRef](#)]
6. Lavagna, L.; Massella, D.; Priola, E.; Pavese, M. Relationship between Oxygen Content of Graphene and Mechanical Properties of Cement-Based Composites. *Cem. Concr. Compos.* **2021**, *115*, 103851. [[CrossRef](#)]
7. Anas, M.; Khan, M.; Bilal, H.; Jadoon, S.; Khan, M.N. Fiber Reinforced Concrete: A Review. In Proceedings of the 12th International Civil Engineering Conference, Karachi, Pakistan, 22 September 2022; p. 3.
8. Lavagna, L.; Bartoli, M.; Pavese, M.; Beldouque Correa, M.C.; Tagliaferro, A.; Hernandez, F.R. Morphed Graphene as Reinforcement for Oil-Well Class G Cement Composites. *Mater. Lett.* **2026**, *404*, 139656. [[CrossRef](#)]
9. Cui, K.; Chang, J.; Feo, L.; Chow, C.L.; Lau, D. Developments and Applications of Carbon Nanotube Reinforced Cement-Based Composites as Functional Building Materials. *Front. Mater.* **2022**, *9*, 861646. [[CrossRef](#)]
10. Konsta-Gdoutos, M.S.; Aza, C.A. Self Sensing Carbon Nanotube (CNT) and Nanofiber (CNF) Cementitious Composites for Real Time Damage Assessment in Smart Structures. *Cem. Concr. Compos.* **2014**, *53*, 162–169. [[CrossRef](#)]
11. Chung, D.D.L. Self-Monitoring Structural Materials. *Mater. Sci. Eng. R Rep.* **1998**, *22*, 57–78. [[CrossRef](#)]
12. Metaxa, Z.S.; Tolkou, A.K.; Efstathiou, S.; Rahdar, A.; Favvas, E.P.; Mitropoulos, A.C.; Kyzas, G.Z. Nanomaterials in Cementitious Composites: An Update. *Molecules* **2021**, *26*, 1430. [[CrossRef](#)]
13. Macías-Silva, M.A.; Cedeño-Muñoz, J.S.; Morales-Paredes, C.A.; Tinizaray-Castillo, R.; Perero-Espinoza, G.A.; Rodríguez-Díaz, J.M.; Jarre-Castro, C.M. Nanomaterials in Construction Industry: An Overview of Their Properties and Contributions in Building House. *Case Stud. Chem. Environ. Eng.* **2024**, *10*, 100863. [[CrossRef](#)]

14. Sobolkina, A.; Mechtcherine, V.; Khavrus, V.; Maier, D.; Mende, M.; Ritschel, M.; Leonhardt, A. Dispersion of Carbon Nanotubes and Its Influence on the Mechanical Properties of the Cement Matrix. *Cem. Concr. Compos.* **2012**, *34*, 1104–1113. [[CrossRef](#)]
15. Lu, D.; Zhong, J. Carbon-Based Nanomaterials Engineered Cement Composites: A Review. *J. Infrastruct. Preserv. Resil.* **2022**, *3*, 2. [[CrossRef](#)]
16. Lavagna, L.; Bartoli, M.; Suarez-Riera, D.; Cagliero, D.; Musso, S.; Pavese, M. Oxidation of Carbon Nanotubes for Improving the Mechanical and Electrical Properties of Oil-Well Cement-Based Composites. *ACS Appl. Nano Mater.* **2022**, *5*, 6671–6678. [[CrossRef](#)]
17. Lavagna, L.; Musso, S.; Ferro, G.; Pavese, M. Cement-Based Composites Containing Functionalized Carbon Fibers. *Cem. Concr. Compos.* **2018**, *88*, 165–171. [[CrossRef](#)]
18. Lavagna, L.; Santagati, A.; Bartoli, M.; Suarez-Riera, D.; Pavese, M. Cement-Based Composites Containing Oxidized Graphene Nanoplatelets: Effects on the Mechanical and Electrical Properties. *Nanomaterials* **2023**, *13*, 901. [[CrossRef](#)]
19. Mansouri Sarvandani, M.; Mahdikhani, M.; Aghabarati, H.; Haghparast Fatmehsari, M. Effect of Functionalized Multi-Walled Carbon Nanotubes on Mechanical Properties and Durability of Cement Mortars. *J. Build. Eng.* **2021**, *41*, 102407. [[CrossRef](#)]
20. Balasubramanian, K.; Burghard, M. Chemically Functionalized Carbon Nanotubes. *Small* **2005**, *1*, 180–192. [[CrossRef](#)]
21. Kuila, T.; Bose, S.; Mishra, A.K.; Khanra, P.; Kim, N.H.; Lee, J.H. Chemical Functionalization of Graphene and Its Applications. *Progress. Mater. Sci.* **2012**, *57*, 1061–1105. [[CrossRef](#)]
22. Qiao, M.; Ran, Q.; Wu, S. Novel Star-like Surfactant as Dispersant for Multi-Walled Carbon Nanotubes in Aqueous Suspensions at High Concentration. *Appl. Surf. Sci.* **2018**, *433*, 975–982. [[CrossRef](#)]
23. Shiba, K.; Tagaya, M.; Samitsu, S.; Motozuka, S. Effective Surface Functionalization of Carbon Fibers for Fiber/Polymer Composites with Tailor-Made Interfaces. *ChemPlusChem* **2014**, *79*, 197–210. [[CrossRef](#)]
24. Ebrahim, A.; Kandasamy, S. The Effect of Using Multi-Walled Carbon Nanotubes on the Mechanical Properties of Concrete: A Review. *Innov. Infrastruct. Solut.* **2023**, *8*, 251. [[CrossRef](#)]
25. Kang, S.-T.; Seo, J.-Y.; Park, S.-H. The Characteristics of CNT/Cement Composites with Acid-Treated MWCNTs. *Adv. Mater. Sci. Eng.* **2015**, *2015*, 308725. [[CrossRef](#)]
26. Wang, B.; Jiang, R.; Wu, Z. Investigation of the Mechanical Properties and Microstructure of Graphene Nanoplatelet-Cement Composite. *Nanomaterials* **2016**, *6*, 200. [[CrossRef](#)]
27. Han, B.; Zhang, L.; Zhang, C.; Wang, Y.; Yu, X.; Ou, J. Reinforcement Effect and Mechanism of Carbon Fibers to Mechanical and Electrically Conductive Properties of Cement-Based Materials. *Constr. Build. Mater.* **2016**, *125*, 479–489. [[CrossRef](#)]
28. Barbhuiya, S.; Chow, P. Nanoscaled Mechanical Properties of Cement Composites Reinforced with Carbon Nanofibers. *Materials* **2017**, *10*, 662. [[CrossRef](#)] [[PubMed](#)]
29. Zhao, Y.; Zhang, J.; Qiang, S.; Lu, H.; Li, J. Effect of Carbon Fibers and Graphite Particles on Mechanical Properties and Electrical Conductivity of Cement Composite. *J. Build. Eng.* **2024**, *94*, 110036. [[CrossRef](#)]
30. Li, L.; Wang, B.; Hubler, M.H. Carbon Nanofibers (CNFs) Dispersed in Ultra-High Performance Concrete (UHPC): Mechanical Property, Workability and Permeability Investigation. *Cem. Concr. Compos.* **2022**, *131*, 104592. [[CrossRef](#)]
31. Pavese, M.; Musso, S.; Bianco, S.; Giorcelli, M.; Pugno, N. An Analysis of Carbon Nanotube Structure Wettability before and after Oxidation Treatment. *J. Phys. Condens. Matter* **2008**, *20*, 474206. [[CrossRef](#)]
32. Zeng, H.; Lai, Y.; Qu, S.; Yu, F. Effect of Graphene Oxide on Permeability of Cement Materials: An Experimental and Theoretical Perspective. *J. Build. Eng.* **2021**, *41*, 102326. [[CrossRef](#)]
33. Qiao, M.; Chen, G.; Fang, Y.; Li, Y.; Shi, M. Interaction Between Air Entraining Agent and Graphene Oxide and Its Effect on Bubble Behavior of Cement-Based Materials. *Buildings* **2025**, *15*, 3631. [[CrossRef](#)]
34. Zeng, H.; Lai, Y.; Qu, S.; Qin, Y. Graphene Oxide-Enhanced Cementitious Materials under External Sulfate Attack: Implications for Long Structural Life. *ACS Appl. Nano Mater.* **2020**, *3*, 9784–9795. [[CrossRef](#)]
35. Zeng, H.; Lai, Y.; Qu, S.; Yu, F. Exploring the Effect of Graphene Oxide on Freeze–Thaw Durability of Air-Entrained Mortars. *Constr. Build. Mater.* **2022**, *324*, 126708. [[CrossRef](#)]
36. Bezerra, M.A.; Santelli, R.E.; Oliveira, E.P.; Villar, L.S.; Escalera, L.A. Response Surface Methodology (RSM) as a Tool for Optimization in Analytical Chemistry. *Talanta* **2008**, *76*, 965–977. [[CrossRef](#)]
37. Leardi, R. Experimental Design in Chemistry: A Tutorial. *Anal. Chim. Acta* **2009**, *652*, 161–172. [[CrossRef](#)]
38. Kumar, R.; Reji, M. Response Surface Methodology (RSM): An Overview to Analyze Multivariate Data. *Indian J. Microbiol. Res.* **2023**, *9*, 241–248. [[CrossRef](#)]
39. Lavagna, L.; Nisticò, R.; Musso, S.; Pavese, M. Functionalization as a Way to Enhance Dispersion of Carbon Nanotubes in Matrices: A Review. *Mater. Today Chem.* **2021**, *20*, 100477. [[CrossRef](#)]
40. Lavagna, L.; Suarez-Riera, D.; Pavese, M. Synergistic Effect of Carbon-Based Reinforcements on the Mechanical Properties of Cement-Based Composites. *J. Compos. Sci.* **2023**, *7*, 430. [[CrossRef](#)]
41. JCI-S-002-2003; Test for Load-Displacement Curve of Fiber Reinforced Concrete by Use of Notched Beam, Tokyo, Japan, 2003.
42. Cox, D.R. Randomization in the Design of Experiments. *Int. Stat. Rev.* **2009**, *77*, 415–429. [[CrossRef](#)]

43. Pethaperumal, S.; Mohanraj, G.T.; Kumar, P.S. Characterization of MWCNT and SWCNT Functionalized by Acid Treatments and the Effect of Functionalized Carbon Nanotubes on Electrical Properties of PMMA-MWCNT and PMMA-SWCNT Nanocomposites. *Appl. Nanosci.* **2023**, *13*, 4167–4176. [[CrossRef](#)]
44. Martincic, M.; Sandoval, S.; Oró-Solé, J.; Tobías-Rossell, G. Thermal Stability and Purity of Graphene and Carbon Nanotubes: Key Parameters for Their Thermogravimetric Analysis (TGA). *Nanomaterials* **2024**, *14*, 1754. [[CrossRef](#)]
45. Dalla, P.T.; Tragazikis, I.K.; Trakakis, G.; Galiotis, C.; Dassios, K.G.; Matikas, T.E. Multifunctional Cement Mortars Enhanced with Graphene Nanoplatelets and Carbon Nanotubes. *Sensors* **2021**, *21*, 933. [[CrossRef](#)] [[PubMed](#)]
46. Abedi, M.; Fangueiro, R.; Gomes Correia, A. Ultra-Sensitive Affordable Cementitious Composite with High Mechanical and Microstructural Performances by Hybrid CNT/GNP. *Materials* **2020**, *13*, 3484. [[CrossRef](#)] [[PubMed](#)]
47. Kanellopoulou, I.; Kartsonakis, I.A.; Chrysanthopoulou, A.I.; Charitidis, C.A. The Effect of Carbon Nanotubes and Carbon Microfibers on the Piezoresistive and Mechanical Properties of Mortar. *Fibers* **2024**, *12*, 62. [[CrossRef](#)]

**Disclaimer/Publisher’s Note:** The statements, opinions and data contained in all publications are solely those of the individual author(s) and contributor(s) and not of MDPI and/or the editor(s). MDPI and/or the editor(s) disclaim responsibility for any injury to people or property resulting from any ideas, methods, instructions or products referred to in the content.